FAULT MODELLING OF THE EARLY-2014 ~M6 EARTHQUAKES IN CEPHALONIA ISLAND (W. GREECE) BASED ON GPS MEASUREMENTS

By

Vassilis Sakkas & Evangelos Lagios

SUPPLEMENTARY SECTION

Table I

Horizontal and Vertical Displacement Components with Error Estimates of Cephalonia–Ithaca GPS Network (2010-2014) (Time Lapse ~3.9 years) (Reference Frame: IGb08)

Station	*E-W (cm)*	σ_{E-W} *(cm)*	*N-S (cm)*	σ_{N-S} *(cm)*	*Up (cm)*	σ_{Up} *(cm)*
01	5.68	0.28	-0.63	0.33	1.87	0.74
02	6.16	0.25	-0.56	0.30	1.70	0.68
03	6.01	0.27	0.45	0.33	2.82	0.73
04	4.09	0.37	1.33	0.46	-0.21	0.61
05	6.05	0.28	-0.86	0.33	1.01	0.73
06	4.68	0.18	0.80	0.21	-3.18	0.27
08	-1.07	0.35	-1.74	0.40	-1.19	0.51
09	-4.49	0.31	-5.47	0.35	-3.13	0.50
10	0.50	0.40	-0.45	0.48	-1.05	1.05
11	-1.62	0.35	-3.39	0.42	-2.72	0.54
12	1.52	0.51	-0.70	0.60	-2.10	0.72
13	3.51	0.38	0.57	0.47	-2.76	0.70
14	-13.36	0.33	-13.36	0.39	-11.49	0.44
15	-9.88	0.28	38.75	0.36	15.40	0.49
16	4.09	0.32	7.88	0.37	13.50	0.51
17	0.46	0.33	15.96	0.39	8.40	0.63
18	3.34	0.30	4.91	0.35	9.20	0.61
19	3.00	0.72	-15.34	0.78	10.60	1.10
20	5.71	0.27	-4.14	0.32	-2.09	0.42
21	7.10	0.29	-1.84	0.34	1.20	0.44
22	6.34	0.28	-0.80	0.33	2.55	0.59
40	6.80	0.49	1.80	0.57	0.30	1.08
51	3.13	0.43	2.11	0.51	1.20	0.91
52	4.23	0.45	1.78	0.53	1.46	1.09
Sara	3.71	0.50	-0.37	0.60	2.86	1.02
VLSM	3.92	0.29	0.35	0.32	-1.18	0.31

Table II

Estimated Horizontal and Vertical Displacement Components with Error Estimates of Cephalonia–Ithaca GPS Network for the Pre-Earthquake Sequence to 2014 Measurement Period (Time Lapse ~1.2 Months) (Reference Frame: IGb08)

Station	*E-W (cm)*	σ_{E-W} *(cm)*	*N-S (cm)*	σ_{N-S} *(cm)*	*Up (cm)*	σ_{Up} *(cm)*
01	-0.18	0.79	-0.86	0.88	3.11	1.68
02	0.22	0.82	-1.18	0.91	2.55	1.73
03	0.00	0.79	-0.36	0.88	3.48	1.68
04	-1.81	0.79	0.55	1.18	0.49	2.26
05	0.04	0.82	-1.48	0.92	1.86	1.75
06	-1.72	0.19	-0.48	0.21	-2.99	0.38
08	-8.02	0.37	-4.03	0.49	-2.00	1.44
09	-11.71	0.41	-7.72	0.48	-3.91	1.33
10	-8.77	0.50	-0.84	0.75	0.04	1.17
11	-8.10	0.54	-4.4	0.61	-2.25	1.14
12	-6.05	0.56	-1.9	1.04	-1.83	1.72
13	-3.36	0.60	-0.21	0.91	-2.06	1.77
14	-20.78	0.37	-15.06	0.44	-11.68	0.87
15	-17.41	0.47	36.69	0.51	14.82	1.23
16	-3.86	0.40	5.36	0.49	12.45	1.53
17	-6.87	0.45	12.58	0.48	6.50	0.99
18	-3.06	0.34	3.62	0.40	7.00	1.28
19	-3.87	0.80	-18.41	0.86	9.01	2.89
20	-1.08	0.31	-6.24	0.35	-2.71	1.19
21	-0.31	0.34	-3.08	0.53	1.43	1.35
22	0.44	0.79	-2.82	0.88	2.01	1.68
40	0.09	1.05	2.58	1.16	2.55	2.52
51	-2.19	1.03	2.34	1.13	2.91	2.48
52	-1.86	0.93	1.16	1.04	2.31	2.11
Sara	-1.33	1.13	0.52	1.17	5.23	2.53
VLSM	-2.53	0.18	-1.20	0.15	-1.14	0.26
KIPO *	-0.11	0.27	7.63	0.31	5.35	0.42
KEFA **	5.50	-	-16.00	-	8.00	-

(*) Period: Sep. 2013 – Feb. 2014.

(**) Vector provided by NTUA (Period: Jan. 25 to Feb.3, 2014).

The Strain Field

The horizontal strain field was calculated on the basis of the horizontal GPS deformation vectors for both Cephalonia and Ithaca (period 2010-2014) using the software after Pesci and Teza (2007). The strain-rate was produced applying a correlation length of 4km and error estimate (σ) of 10mm. Two different strain maps were compiled: (i) Figure 1a which takes into consideration only the sites located on Paliki and those on the western part of the main island; (ii) Figure 1b which assumes all stations of the GPS network. These results show that extension takes place basically at a NW-SE direction, consistent with the strike-slip character of the activated faulting zones. Compression is noticed in the vicinity of the northern part of Paliki (Fig. 1a), mainly being controlled by the stations 14, 15 and 16. It is noted that moving away from the activated area, the amplitude of the principal strain component decreases almost by an order of magnitude (Fig. 1b). Towards Ithaca, the extensional components rotate to an almost E-W direction, marking the migration of Ithaca eastwards.

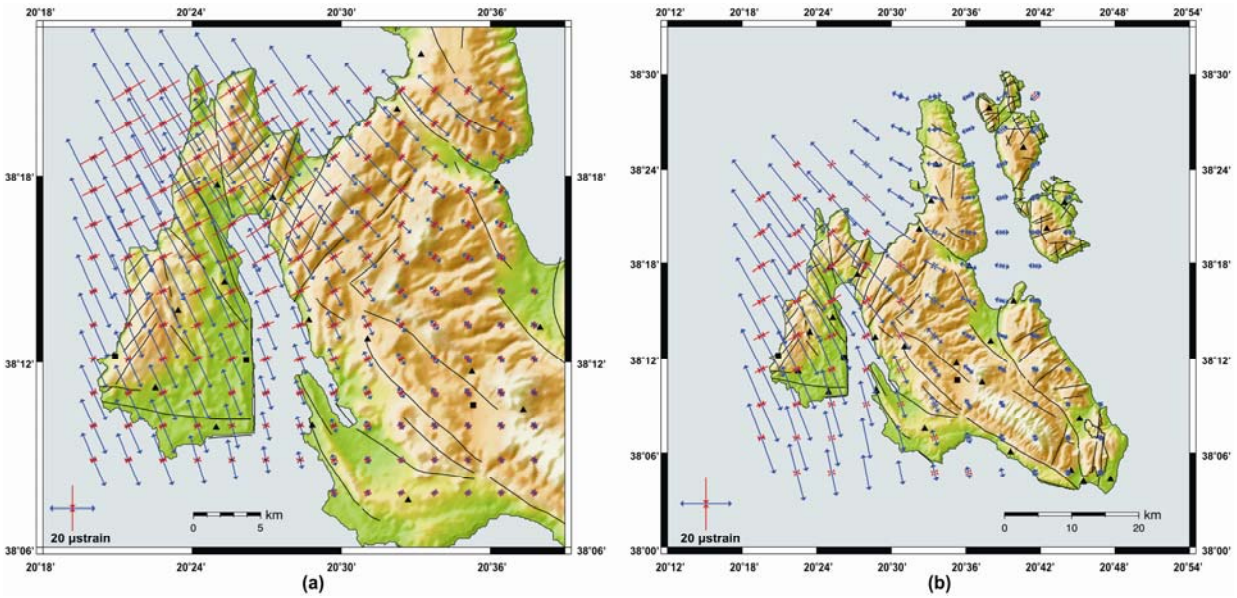

Figure 1 **(a)** Strain Field in Paliki and adjacent area; **(b)** Strain Field of Cephalonia-Ithaca islands.

***Double Fault* Model**

A checkerboard resolution test for the adopted *double fault* approach was performed. The fault planes were divided into 4km x 4km and 3.3km x 3.3km uniform patches for the southern (AB) and northern (CD) fault, respectively (Fig. 2). Similarly, as the *single fault* scenario, better resolution was achieved for the shallower patches, while the resolution fades away for depths greater than 16km and 14km for the southern and northern fault, respectively.

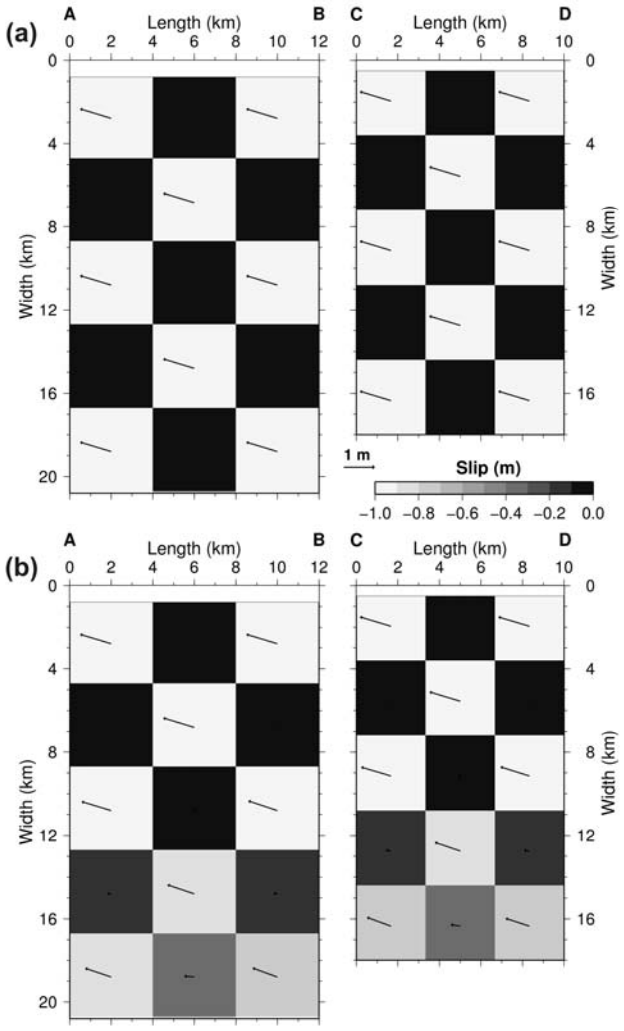

Figure 2. Checkerboard resolution test of the GPS network on the fault planes slip distribution. **(a)** Synthetic input slip distribution; **(b)** Output best-fit slip distribution at *k*=100 inverted from the synthetic surface deformation. Arrows represent the resultant of the Dip and Slip distribution along the planes. The grey scale indicates only the slip variation. Synthetic fault planes have the same geometric parameters as the *double fault* model.

The *double fault* model was examined also for larger burial depths. Burial depths of 1.8km and 1.3km for the southern and northern fault, respectively, resulted to an acceptable misfit on the stations located in Paliki, but with a considerable better misfit for the stations east of Paliki (Fig. 3). The latter is an indication that a significant amount of aftershock deformation component is inherent in the stations at Paliki.

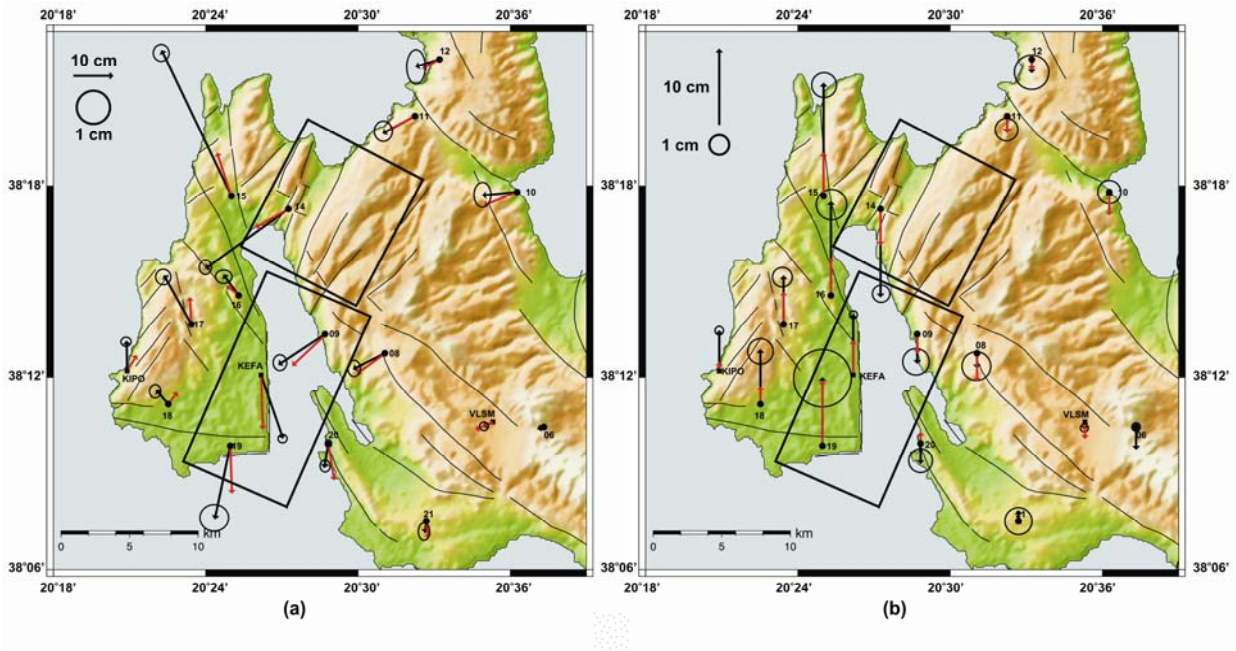

Figure 3. (a) Horizontal, and (**b**) Vertical fitting of the double *fault* model for *k*=2000, and burial depth of 1.8km and 1.3km for the southern and northern fault, respectively. Rectangles indicate the fault planes projected on the ground surface. Black and Red arrows indicate the observed and calculated vectors, respectively.

Spatial distribution of the ground displacement (Fig. 4a) revealed a pattern of deformation similar to the pattern observed for shallower burial depths of smaller amplitudes. The planes of the two faults (Fig. 4b) show a uniform, but intense and extensive slip on their surface. The rupture plane of the southern fault extends to depth of about 22km, while the northern fault extends to more than 18km depths, considerably deeper than the hypocentral depth of the Mw=5.9 seismic event. The former implies that the modelling procedure (in order to fit the observed data) increases the area of rupture and the amplitude of slip, as the burial depth increases, at an attempt to fit the large amplitude deformation vectors observed in Paliki. It has to be noticed here that the adopted burial depth of 1.8km and 1.3km was found to be the maximum depth with acceptable fit between observed and calculated data. The *k* factor for this *double fault* model was selected to be 2000 (Fig. 4c) with an overall RMS misfit of 0.063m. A mean slip of -0.47m and -0.32m, together with a mean dip-thrust component of +0.05m and +0.12m was calculated for the southern and northern fault, respectively.

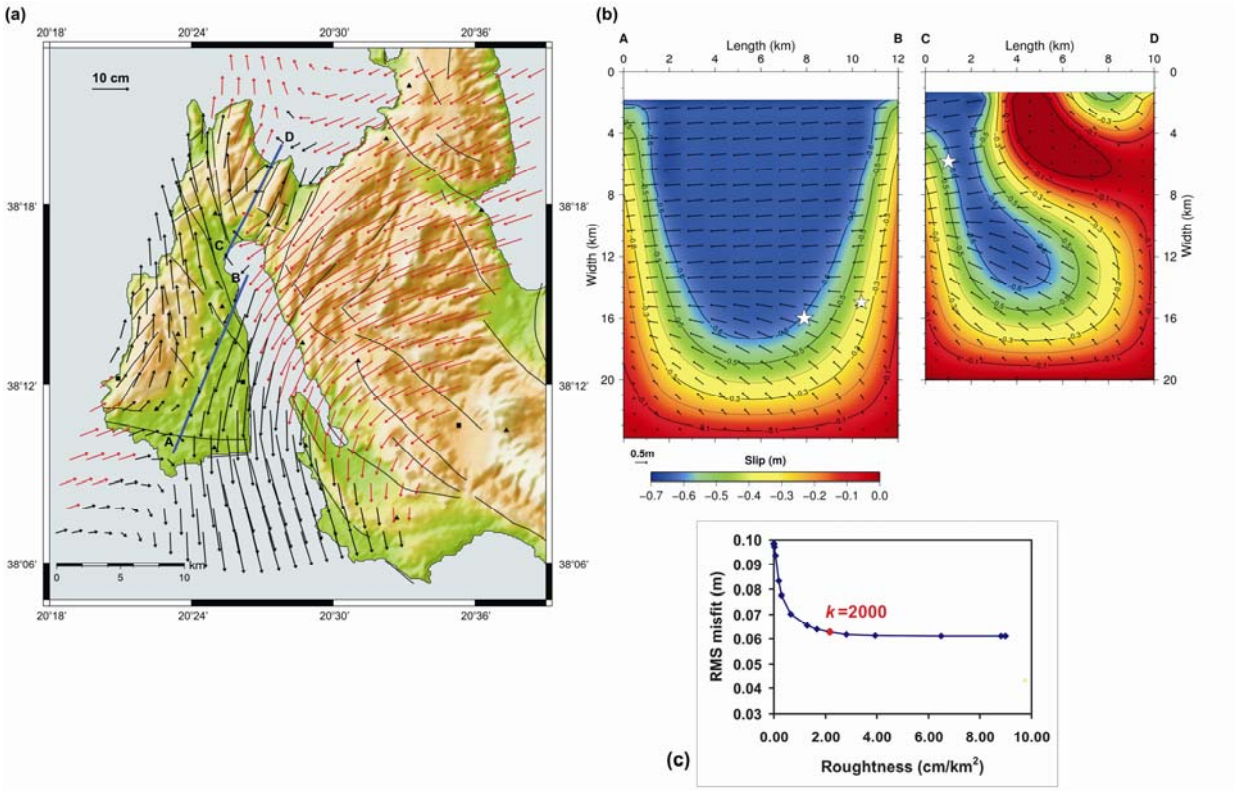

Figure 4. **(a)** Horizontal spatial deformation for the *double fault* model (Blue Line) for burial depths 1.8km and 1.3km of the southern and northern fault, respectively. Red and black arrows indicate areas where a *qualitative* Subsidence and Uplift takes place. **(b)** Slip distribution on the planes of the *double fault* model discretized at 1km x 1km patches for *k*=2000. Arrows represent the resultant of the Dip and Slip distribution along the planes. The coloured scale indicates only the slip variation. White stars represent the horizontal projection on the plane of the three seismic events. (**c**) The trade-off curve between decreased Roughness (increased smoothing) and increased RMS misfit for *double fault* model. The preferred model at *k*=2000 is chosen balancing the trade-off between misfit and smoothing.

Reference

Pesci A., Teza G., 2007. Strain rate analysis over the central Apennines from GPS velocities: the development of a new free software. Bollettino di Geodesia e Scienze Affini 56, 69-88.